Charge Carrier Transporting, Photoluminescent, and Electroluminescent Properties of Zinc(II)-2-(2-hydroxyphenyl)benzothiazolate Complex

Xinjun Xu,[†] Yi Liao,[‡] Gui Yu,*[,†] Han You,[§] Chong'an Di,[†] Zhongmin Su,*[,‡] Dongge Ma,[§] Qian Wang,[⊥] Shayu Li,[⊥] Shuangqing Wang,[⊥] Jianping Ye,[⊥] and Yunqi Liu*[,†]

Beijing National Laboratory for Molecular Sciences, Key Laboratory of Organic Solids, Institute of Chemistry, Chinese Academy of Sciences, Beijing 100080, People's Republic of China, Institute of Functional Material Chemistry, Faculty of Chemistry, Northeast Normal University, Changchun 130024, People's Republic of China, Key State Laboratory of Polymer Physics and Chemistry, Changchun Institute of Applied Chemistry, Chinese Academy of Sciences, Changchun 130022, People's Republic of China, and Key Laboratory of Photochemistry, Institute of Chemistry, Chinese Academy of Sciences, Beijing 100080, People's Republic of China

Received December 13, 2006. Revised Manuscript Received February 5, 2007

Zinc(II)-2-(2-hydroxyphenyl)benzothiazolate complex is an excellent white-light-emitting material. Despite some studies devoted to this complex, no information on the real origin of the unusually broad electroluminescent (EL) emission is available. Therefore, we investigate photoluminescent and EL properties of the zinc complex. Orange phosphorescent emission at 580 nm was observed for the complex in thin film at 77 K, whereas only fluorescent emission was obtained at room temperature. Molecular orbitals, excitation energy, and emission energy of the complex were investigated using quantum chemical calculations. We fabricated the device with a structure of ITO/F_{16}CuPc(5.5 nm)/Zn-complex/Al, where F_{16}CuPc is hexadecafluoro copper phthalocyanine. The EL spectra varied strongly with the thickness of the emissive layer. We observed a significant change in the emission spectra with the viewing angles. Optical interference effects and light emission originating both from fluorescence and from phosphorescence can explain all of the observed phenomena, resulting in the broad light emission for the devices based on the Zn complex. We calculated the charge transfer integral and the reorganization energy to explain why the Zn complex is a better electron transporter than a hole transporter.

Introduction

White organic light-emitting diodes (WOLEDs) have attracted much attention due to their potential application in flat-panel displays and lighting sources.[1] Several strategies have been used to fabricate WOLEDs.[2] These include the manufacture of the multilayer devices by consecutive evaporation or co-evaporation of different light-emitting compounds and the single-layer polymer blend devices. In these devices, the simultaneous excitation of different molecular species gives rise to light emission with different primary colors of visible light that combine to give white light. However, problems such as color dependence on the driving voltage and undesired Förster-type energy transfer between chromophores exist in such devices. Furthermore, in both the multilayer organic devices and single-layer polymer ones, the emission color is usually sensitive to the device structure parameters such as the active layer thickness and doping concentration, and to the driving voltage. In addition, the white-light emission can also be obtained from excimers and/or exciplexes of the organic or polymer chromophores. Unfortunately, they have not produced satisfactory white-light emission in terms of color and efficiency. Most of the above problems seem to be avoidable if a single-component material can be used as the emitting species. Early in 1997, Yang reported white-light emission from a single-component device in which the polyfluorene derivative was used as the emitter.[3] Single-component polymeric materials prepared from anthracene-fused norbornadiens through ring-opening metathesis polymerization process was also used to fabricate the white devices in which the broad emission band was composed of a blue emission

* Corresponding authors. E-mail: yugui@mail.iccas.ac.cn; liuyq@mail.iccas.ac.cn.

[†] Key Laboratory of Organic Solids, Institute of Chemistry, Chinese Academy of Sciences.

[‡] Northeast Normal University.

[§] Changchun Institute of Applied Chemistry, Chinese Academy of Sciences.

[⊥] Key Laboratory of Photochemistry, Institute of Chemistry, Chinese Academy of Sciences.

(1) (a) D'Andrade, B. W.; Forrest, S. R. *Adv. Mater.* **2004**, *16*, 1585. (b) Mazzeo, M.; Pisignano, D.; Della Sala, F.; Thompson, J.; Blyth, R. I. R.; Gigli, G.; Cingolani, R.; Sotgiu, G.; Barbarella, G. *Appl. Phys. Lett.* **2003**, *82*, 334. (c) Huang, J. S.; Li, G.; Wu, E.; Xu, Q. F.; Yang, Y. *Adv. Mater.* **2006**, *18*, 114. (d) Jiang, J. X.; Xu, Y. H.; Yang, W.; Guan, R.; Liu, Z. Q.; Zhen, H. Y.; Cao, Y. *Adv. Mater.* **2006**, *18*, 1769. (e) Tu, G. L.; Mei, C. Y.; Zhou, Q. G.; Cheng, Y. X.; Geng, Y. H.; Wang, L. X.; Ma, D. G.; Jing, X. B.; Wang, F. S. *Adv. Funct. Mater.* **2006**, *16*, 101.

(2) (a) Wang, L. D.; Lei, G. T.; Qiu, Y. *J. Appl. Phys.* **2005**, *97*, 114503. (b) Cheng, J. A.; Chen, C. H. *J. Mater. Chem.* **2005**, *15*, 1179. (c) D'Andrade, B. W.; Brooks, J.; Adamovich, V.; Thompson, M. E.; Forrest, S. R. *Adv. Mater.* **2002**, *14*, 1032. (d) Sun, Q. J.; Fan, B. H.; Tan, Z. A.; Yang, C. H.; Li, Y. F.; Yang, Y. *Appl. Phys. Lett.* **2006**, *88*, 163510. (e) Zhang, Y. F.; Cheng, G.; Zhao, Y.; Hou, J. Y.; Liu, S. Y. *Appl. Phys. Lett.* **2005**, *86*, 011112.

(3) Yang, Y.; Pei, Q. B. *J. Appl. Phys.* **1997**, *81*, 3294.

10.1021/cm062960b CCC: $37.00
Published on Web 03/09/2007

from anthracene and a red one from aggregates.[4] Another single emitting component polymer white device was achieved with the blue-green emission coming from the individual lumophore and excimer and the red emission originating from the electromer.[5] Recently, Wang and co-workers reported a strategy to realize white electroluminescence (EL) with simultaneous blue, green, and red emission from a single polymer.[6] Simultaneously, a few single-emitting component WOLEDs have been described.[7] Lee and co-workers reported efficient single-emitting component WOLEDs based on 1,3,5-tris(2-(9-ethylcarbazyl-3)ethylene)-benzene.[7a] The white-light emission consists of three components: fluorescence, phosphorescence, and electromer emission. This device, with a small change in emission color with respect to the driving voltage, offers definite advantages over the multicomponent organic and single-layer blended polymer white-light-emitting devices, whose emission color shows substantial voltage dependence. Nevertheless, WOLEDs made by single-emitting component usually suffer from a low efficiency. Therefore, the search for new organic light-emitting materials used in single-emitting component WOLEDs is of obvious interest and importance.

Organic and polymeric light-emitting materials can be divided into two general classes that are fluorescent and phosphorescent. From spin statistics, theoretical calculations, and experiment, the singlet:triplet exciton ratio is 1:3, limiting a maximum internal EL efficiency from the fluorescent materials to $\leq$25%. Unlike fluorescence, phosphorescence makes use of both the singlet and triplex excited states, suggesting potential for reaching the maximum internal efficiency of 100%. Emission of the most organic compounds is dominated by fluorescence, while their phosphorescent emission is usually very weak. One effective way of promoting phosphorescent emission from the organic molecules is to introduce transition metal centers into the organic ligands, where the strong spin−orbit coupling caused by heavy metal ions results in efficient intersystem crossing from the singlet to triplet excited states and phosphorescent emission. A recent breakthrough using phosphorescent lumophores has demonstrated an ability to make highly efficient EL devices. The electrophosphorescent materials for organic light-emitting diode (OLED) fabrication are mainly cyclometalated complexes of Ir(III), Re(I), Ru(II), Os(II), and Pt(II), whose high cost leads to high-cost products for large-area display applications.[8] A more efficient way for cost reduction is replacing the above complexes with less expensive metal complexes as the emissive materials in OLEDs. Only a few examples of relatively abundant, inexpensive, and nontoxic metal complexes have been reported. Ma et al. fabricated OLEDs with a tetranuclear Cu(I) complex;[9] however, the reported efficiency of 0.1% is still much lower than that of the Pt(II) and Ir(III) complexes. Recently, phosphorescent OLEDs based on the mononuclear Cu(I) complexes exhibit a highly current efficiency up to 10.5 cd/A, which is comparable to that of the Ir(III) complexes in similar device structures.[10] Wang and co-workers reported a phosphorescent zinc complex with intense blue emission, whereas the EL properties have not been reported.[11] Therefore, it is possible to obtain electrophosphorescent emission of Zn complexes.

Zinc(II)-2-(2-hydroxyphenyl)benzothiazolate complex has been studied as an excellent white EL material.[12] In a previous paper, we demonstrate that the dimeric molecules $[Zn(BTZ)_2]_2$ exist in the single crystal prepared by a train sublimation method.[13] To date, reasonable explanation of the unusually broad white-light emission has not yet been reported. We anticipate that this could offer us an opportunity to elucidate the origin of the unique optoelectronic properties of the complex. In this work, we investigate in detail the photoluminescent (PL) and EL characteristics and carry out related theoretical calculations. For the sake of extensive explanation of the reason why the dimer $[Zn(BTZ)_2]_2$ exhibits an higher electron mobility than hole mobility, the theoretical study of the transport properties was performed.

The photophysical properties of $[Zn(BTZ)_2]_2$ were studied using experimental measurements and theoretical calculations. We observed a phosphorescent emission from the $[Zn(BTZ)_2]_2$ film at 77 K. The stronger optical absorption, fluorescent emission, and phosphorescent emission mainly correspond to the charge transition between the ligands, whereas the contribution from the Zn^{2+} ions appears to be distinctly small. A broad EL spectrum with a full-width at half-maximum (fwhm) of 220 nm was obtained for the device ITO/F_{16}CuPc(5.5 nm)/$[Zn(BTZ)_2]_2$/Al, where F_{16}CuPc is hexadecafluoro copper phthalocyanine. We demonstrated the broad light-emission results from the optical interference effects and light emission originating from both fluorescence and phosphorescence.

(4) Tsai, M. L.; Liu, C. Y.; Hsu, M. A.; Chow, T. J. *Appl. Phys. Lett*. **2003**, *82*, 550.
(5) Lee, Y. Z.; Chen, X.; Chen, M. C.; Chen, S. A. *Appl. Phys. Lett*. **2001**, *79*, 308.
(6) Liu, J.; Zhou, Q. G.; Cheng, Y. X.; Geng, Y. H.; Wang, L. X.; Ma, D. G.; Jing, X. B.; Wang, F. S. *Adv. Mater*. **2005**, *17*, 2974.
(7) (a) Li, J. Y.; Liu, D.; Ma, C.; Lengyel, O.; Lee, C. S.; Tung, C. H.; Lee, S. T. *Adv. Mater*. **2004**, *16*, 1538. (b) Mazzeo, M.; Vitale, V.; Sala, F. D.; Anni, M.; Barbarella, G.; Favaretto, L.; Sotgiu, G.; Cingolani, R.; Gigli, G. *Adv. Mater*. **2005**, *17*, 34. (c) Liu, Y.; Nishiura, M.; Wang, Y.; Hou, Z. M. *J. Am. Chem. Soc*. **2006**, *128*, 5592.
(8) (a) Baldo, M. A.; O'Brien, D. F.; You, Y.; Shoustikov, A.; Sibley, S.; Thompson, M. E.; Forrest, S. R. *Nature* **1998**, *395*, 151. (b) Baldo, M. A.; Lamansky, S.; Burrows, P. E.; Thompson, M. E.; Forrest, S. R. *Appl. Phys. Lett*. **1999**, *75*, 4. (c) Baldo, M. A.; Thompson, M. E.; Forrest, S. R. *Nature* **2000**, *403*, 750. (d) Liu, C. Y.; Bard, A. J. *J. Am. Chem. Soc*. **2002**, *124*, 4190. (e) Rudmann, H.; Shimada, S.; Rubner, M. F. *J. Am. Chem. Soc*. **2002**, *124*, 4918. (f) Kwong, R. C.; Lamansky, S.; Thompson, M. E. *Adv. Mater*. **2000**, *12*, 1134. (g) Wu, A.; Yoo, D.; Lee, J.-K.; Rubner, M. F. *J. Am. Chem. Soc*. **1999**, *121*, 4883. (h) Hurley, D. J.; Tor, Y. *J. Am. Chem. Soc*. **2003**, *124*, 3749. (i) Tsuboyama, A.; Iwawaki, H.; Furugori, M.; Mukaide, T.; Kamatani, J.; Igawa, S.; Moriyama, T.; Miura, S.; Takiguchi, T.; Okada, S.; Hoshino, M.; Ueno, K. *J. Am. Chem. Soc*. **2003**, *125*, 12971. (j) Hay, P. J. *J. Phys. Chem. A* **2002**, *106*, 1634.
(9) (a) Ma, Y. G.; Chan, W. H.; Zhou, X. M.; Che, C. M. *New. J. Chem*. **1999**, *23*, 263. (b) Ma, Y. G.; Che, C. M.; Chao, H. Y.; Zhou, X. M.; Chan, W. H.; Shen, J. C. *Adv. Mater*. **1999**, *11*, 852.
(10) Zhang, Q. S.; Zhou, Q. G.; Cheng, Y. X.; Wang, L. X.; Ma, D. G.; Jing, X. B.; Wang, F. S. *Adv. Mater*. **2004**, *16*, 432.
(11) Liu, Q. D.; Wang, R. Y.; Wang, S. N. *Dalton Trans*. **2004**, 2073.
(12) (a) Hamada, Y.; Sano, T.; Fujii, H.; Nishio, Y.; Takahashi, H.; Shibata, K. *Jpn. J. Appl. Phys*. **1996**, *35*, L1339. (b) Sano, T.; Nishio, Y.; Hamada, Y. J.; Takahashi, H.; Usiki, T.; Shibata, K. *J. Mater. Chem*. **2000**, *10*, 157.
(13) Yu, G.; Yin, S. W.; Liu, Y. Q.; Shuai, Z. G.; Zhu, D. B. *J. Am. Chem. Soc*. **2003**, *125*, 14816.

Experimental Section

Computation Method. Geometry optimization for the $[Zn(BTZ)_2]_2$ molecule was completed using the Gaussian 03 software package[14] with the density functional theory. All open-shell calculations were performed using unrestricted methods (UDFT), and spin contamination in the radical species was found to be very small ($\langle S^2 \rangle \leq 0.77$). Becke's three parameters hybrid method[15] using the Lee−Yang−Parr correlation functional[16] was employed (denoted as B3LYP) here. Gradient optimizations were carried out using the 3-21G* basis set for C and H atoms and the 6-31G* basis set for Zn, O, N, and S.

The geometry optimization of the first singlet excited state (S_1) was carried out using time-dependent density-functional formalism (TDDFT)[17] with the B3LYP functional in conjunction with a def-SV(P) basis set, as implemented in TURBOMOLE 5.6.[18] At the first triplet excited state (T_1), direct spin-unrestricted density functional theory (UDFT) calculations using the B3LYP functional with LANL2DZ basis sets were performed. The spin contamination due to the use of unrestricted open shell methodology was found to be very low, where the maximum deviation from the actual value of $S(S+1) = 2$ was not exceeding 0.05. This finding leads to a conclusion that the DFT calculations represent the T_1 state with negligible contamination from the other multiplet states.

On the basis of ground- and excited-state optimization, TD-DFT approach[19] (Gaussian03) was applied to investigate the excited-state electronic properties of complex $[Zn(BTZ)_2]_2$ at the level of TD-B3LYP. This method is based on the Kohn−Sham formulation of DFT and uses the eigenvalues and eigenvectors of the Kohn−Sham equation.

Light-Emitting Device Preparation. Zinc(II)-2-(2-hydroxyphenyl)benzothiazolate complex was synthesized from the complex reaction between zinc acetate dihydrate and 2-(2-hydroxyphenyl)-benzothiazole.[13] Figure 1 shows the molecular structure of the Zn complex. *N*,*N*′-Diphenyl-*N*,*N*′-bis(1-naphenyl)-1,1′-biphenyl-4,4′-diamine (NPB) and tris(8-hydroxyquinolinolato)aluminum (Alq_3) (purchased from Aldrich Chemical Co.) were purified by thermal sublimation. The devices were fabricated on a glass substrate coated with indium tin oxide (ITO, sheet resistance = 30 Ω/sq) using conventional vacuum vapor deposition in a vacuum of 2×10^{-4} Pa. The effective size of the EL devices was 4 mm^2. The organic layers were deposited by means of conventional vacuum deposition. Finally, aluminum was evaporated as a cathode. A quartz crystal oscillator placed near the substrate was used to determine the thickness of each layer, which were calibrated ex situ using an Ambios Technology XP-2 surface profilometer. The absorption and PL spectra were measured with a general TU-1201 UV−vis spectrophotometer and an Hitachi F-4500 fluorescence spectrophotometer, respectively. The fluorescence lifetime was measured on a Horiba NAES-1100 time-resolved spectrofluorometer with a single-photon counting system at room temperature. Phosphorescent lifetime measurements were performed by an Edinburgh Instruments Ltd. FLS-920 time-resolved spectrometer at 77 K. The excited source was the unfocused third harmonic (355 nm, 7 ns pulse width) output of an Nd:YAG laser (Continuum surelite II), and the probe light source was a pulse-xenon lamp. EL spectra and chromaticity coordinates were measured with a SpectraScan PR 650 photometer. Current−voltage−luminance measurements were made simultaneously using a Hewlett-Packard 4140B semiconductor parameter analyzer and a Newport multifunction 2835-C optical meter. The measurements for devices were performed under ambient atmosphere at room temperature.

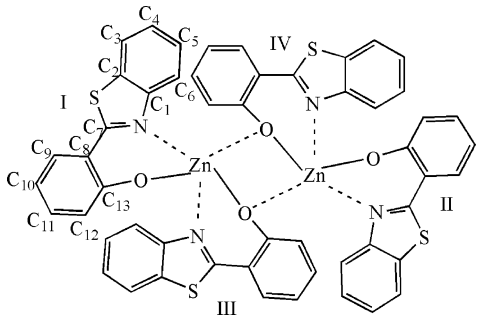

Figure 1. Molecular structures of the Zn complex with labels I−IV designating the four different ligands.

Results and Discussion

Optical Absorption and Photoluminescent Spectra. The photophysical properties including absorption and fluorescent characteristics of $[Zn(BTZ)_2]_2$ have been studied.[12,20] Unfortunately, the phosphorescent properties of $[Zn(BTZ)_2]_2$ have not been reported to the best of our knowledge. Figure 2 shows the room-temperature absorption, fluorescent, and 77 K phosphorescent spectra of $[Zn(BTZ)_2]_2$ in the solution and thin film. The solution of $[Zn(BTZ)_2]_2$ exhibits an absorption maximum at 333 nm to the accompaniment of a shoulder peak at 347 nm. The absorption bands in the 250−380 nm range can be assigned to intraligand ($\pi-\pi^*$) transitions. Upon irradiation by UV−light at room temperature, the $[Zn(BTZ)_2]_2$ solution shows a blue emission with a peak at 455 nm, while the ligand exhibits a green one at 517 nm. Therefore, we suggest that coordination of the ligand with the zinc ion results in a blue shift of emission spectra in contrast to the usual red shift observed for most of the complexes. Manoharan and co-workers have also reported a similar phenomenon.[20a] The theoretical calculation indicates that the main fluorescent emission of $[Zn(BTZ)_2]_2$ corresponds not to the transition from the lowest unoccupied

(14) Frisch, M. J.; Trucks, G. W.; Schlegel, H. B.; Scuseria, G. E.; Robb, M. A.; Cheeseman, J. R.; Montgomery, J. A., Jr.; Vreven, T.; Kudin, K. N.; Burant, J. C.; Millam, J. M.; Iyengar, S. S.; Tomasi, J.; Barone, V.; Mennucci, B.; Cossi, M.; Scalmani, G.; Rega, N.; Petersson, G. A.; Nakatsuji, H.; Hada, M.; Ehara, M.; Toyota, K.; Fukuda, R.; Hasegawa, J.; Ishida, M.; Nakajima, T.; Honda, Y.; Kitao, O.; Nakai, H.; Klene, M.; Li, X.; Knox, J. E.; Hratchian, H. P.; Cross, J. B.; Adamo, C.; Jaramillo, J.; Gomperts, R.; Stratmann, R. E.; Yazyev, O.; Austin, A. J.; Cammi, R.; Pomelli, C.; Ochterski, J. W.; Ayala, P. Y.; Morokuma, K.; Voth, G. A.; Salvador, P.; Dannenberg, J. J.; Zakrzewski, V. G.; Dapprich, S.; Daniels, A. D.; Strain, M. C.; Farkas, O.; Malick, D. K.; Rabuck, A. D.; Raghavachari, K.; Foresman, J. B.; Ortiz, J. V.; Cui, Q.; Baboul, A. G.; Clifford, S.; Cioslowski, J.; Stefanov, B. B.; Liu, G.; Liashenko, A.; Piskorz, P.; Komaromi, I.; Martin, R. L.; Fox, D. J.; Keith, T.; Al-Laham, M. A.; Peng, C. Y.; Nanayakkara, A.; Challacombe, M.; Gill, P. M. W.; Johnson, B.; Chen, W.; Wong, M. W.; Gonzalez, C.; Pople, J. A. *Gaussian 03*, Revision B.04; Gaussian, Inc.: Pittsburgh, PA, 2003.
(15) Becke, A. D. *J. Chem. Phys.* **1993**, *98*, 5648.
(16) Lee, C.; Yang, W.; Parr, R. G. *Phys. Rev. B* **1988**, *37*, 785.
(17) Van Caillie, C.; Amos, R. D. *Chem. Phys. Lett.* **1999**, *308*, 249.
(18) Ahlrichs, R.; Bär, M.; Baron, H.-P.; Bauernschmitt, R.; Böcker, S.; Ehrig, M.; Eichkorn, K.; Elliot, S.; Haase, F.; Häser, M.; Horn, H.; Huber, C.; Huniar, U.; Kattannek, M.; Kölmel, C.; Kollwitz, M.; Ochsenfeld, C.; Öhm, H.; Schäfer, A.; Schneider, U.; Treutler, O.; von Arnim, M.; Weigend, F.; Weis, P.; Weiss, H. *Turbomole*, version 5.6; Quantum Chemistry Group, University of Karlsruhe: Karlsruhe, Germany, 2002.
(19) Casida, M. K.; Jamorski, C.; Casida, K. C.; Salahub, D. R. *J. Chem. Phys.* **1998**, *108*, 4439.
(20) (a) Qureshi, M.; Manoharan, S. S.; Singh, S. P.; Mahapatra, Y. N. *Solid State Commun.* **2005**, *133*, 305. (b) Singh, S. P.; Mohapatra, Y. N.; Qureshi, M.; Manoharan, S. S. *Synth. Met.* **2005**, *155*, 376.

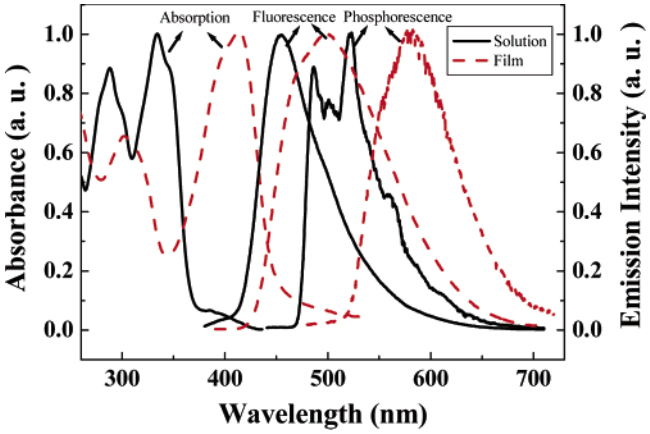

Figure 2. Absorption, fluorescent, and phosphorescent emission spectra of $[Zn(BTZ)_2]_2$ in the solution and thin film.

molecular orbitals (LUMOs) to the highest occupied molecular orbitals (HOMOs) but rather to the transition from LUMO to HOMO-2. This result would be one of the main reasons that coordination of the ligand with the zinc ion gives rise to the blue shift of emission spectra. The emission at 455 nm for $[Zn(BTZ)_2]_2$ decays biexponentially with lifetimes of ca. 0.238 and 3.68 ns, indicating that it arises from fluorescent emission of the singlet excited states. In comparison with those in solution, the absorption and emission spectra of the ligand films is obviously red shift. As a general trend, we observed a progressive red shift of the most intense absorption band and emission peak of the complex when going from the diluted solution to the solid state. The longest absorption band of the complex $[Zn(BTZ)_2]_2$ shifts from 335 nm in the solution to 413 nm in the thin film, while the emission peak shifts from 450 nm in the solution to 496 nm in the thin film. Meanwhile, we observed a shoulder peak at 469 nm for the $[Zn(BTZ)_2]_2$ films. This implies that these molecules in solution exhibit an intermolecular interaction weaker than that in the solid states. At room temperature, the complex in the thin films shows a fluorescent emission with emission lifetimes of 0.89 and 6.27 ns. We obtained phosphorescent emission for the complex both in the thin film and solution at 77 K rather than at room temperature. Orange phosphorescent emission at 580 nm was observed for the complex in thin film at 77 K. The emission decays biexponentially with lifetimes of ca. 0.69 and 2.3 μs. We can consider that the emission of the complex is ligand-based, involving the most likely $\pi-\pi^*$ transitions. This deduction has been determined by following theoretical calculation. The phosphorescent emission of most zinc complexes is usually very weak.

Ground, Excited-Singlet, and Excited-Triplet State Geometries of $[Zn(BTZ)_2]_2$. The photophysical properties, especially the absorption spectra and emissive characteristics, are key factors for determining the EL properties of the organic materials. These characteristics depend mainly on the ground- and excited-state properties of the organic molecules. Therefore, gaining insight into the optoelectronic processes requires a firm knowledge of the molecular properties that can be obtained via quantum chemical calculation. The majority of the work carried out thus far has been on the ground- and excited-state characteristics of

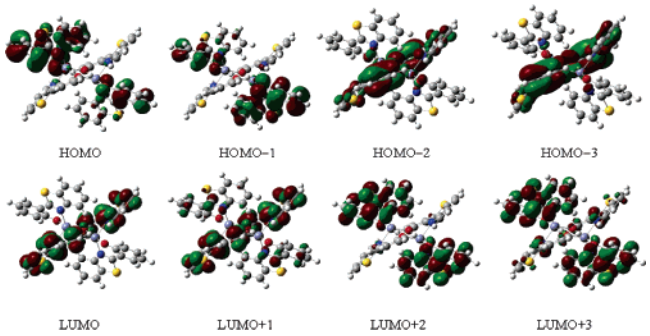

Figure 3. Frontier molecular orbitals for the S_0 state of the $[Zn(BTZ)_2]_2$ molecule.

Alq_3 and Ir complexes.[21] Nevertheless, theoretical calculation on the excited-triplet state of the complexes with photoluminescence originating from the ligands has not been reported. To explore the real origin of the photophysical properties, we calculated the ground, excited-singlet, and excited-triplet states of the $[Zn(BTZ)_2]_2$ complex. Two zinc ions have the same coordination geometries. Both the ligands I and II are bound to one of the Zn atoms only, while the remaining two ligands III and IV are involved in bridging through the phenolato oxygens. Table S1 in the Supporting Information summarizes the optimized bond lengths of the ground (S_0), S_1, and T_1 states of the $[Zn(BTZ)_2]_2$ complex. The S_0 geometry of $[Zn(BTZ)_2]_2$ is in excellent agreement with the experimental values determined in the X-ray structure. HOMOs and LUMOs of $[Zn(BTZ)_2]_2$ largely preserve the electronic structure of the individual 2-(2-hydroxyphenyl)benzothiazole ligands with little contribution from the central zinc atoms. Similar results have been obtained for the molecular orbitals of Alq_3, which are mainly dominated by orbitals originating from the 8-hydroxyquinoline ligands.[21a,b] In agreement with previous DFT works,[13] the HOMO and LUMO orbitals of $[Zn(BTZ)_2]_2$ are strongly localized on the phenoxide ring of the two nonbridging ligands and on the two bridging ligands, respectively. For the S_1 state of $[Zn(BTZ)_2]_2$, the two zinc ions have the same coordination geometries, bond lengths, and bond angles, while the ligands I and II or the ligands III and IV exhibit almost identical bond lengths and bond angles. We found that the two Zn^{2+} ions of the T_1 state as well as the four ligands show different bond lengths and bond angles.

Molecular Orbitals, Excitation Energy, and Emission Energy. We calculated the absorption and emission wavelengths as well as the frontier molecular orbitals (FMOs) for the $[Zn(BTZ)_2]_2$ molecule using the optimized geometries of the S_0, S_1, and T_1 states, respectively. The calculated absorption, fluorescent emission, and phosphorescent emission wavelengths were obtained by using TD-B3LYP. The FMO distribution of the S_0 state is shown in Figure 3. The FMOs are primarily dominated by the orbitals originating from those of the ligands in the complex. The contribution from the Zn^{2+} ions appears to be distinctly small. The HOMO and HOMO−1 are mainly localized on the two nonbridging ligands I and II, whereas both the HOMO−2 and HOMO−3

(21) (a) Curioni, A.; Boero, M.; Andreoni, W. *Chem. Phys. Lett*. **1998**, *294*, 263. (b) Halls, M. D.; Schlegel, H. B. *Chem. Mater*. **2001**, *13*, 2632. (c) Hay, P. J. *J. Phys. Chem. A* **2002**, *106*, 1634.

Table 1. Selected Calculated Excitation Energies (*E*), Wavelengths (*λ*), and Oscillator Strengths (×c4) for Low-Lying Singlet (S_n) States of the $[Zn(BTZ)_2]_2$ Molecule

state	composition[a]	ΔE(eV)/λ(nm)	expl (nm)	*f*
S_1	HO → LU (23%) HO−1 → LU (48%) HO → LU+1 (45%)	2.979/416		0.0005
S_8	HO → LU+2 (45%) HO−2 → LU (44%) HO−1 → LU+3 (24%)	3.407/363.9	347	0.141
S_{10}	HO−1 → LU+3 (48%) HO−2 → LU (43%)	3.420/362.6	347	0.1762
S_{14}	HO−3 → LU+1 (64%)	3.676/337.28	335	0.1631

[a] HO and LO denote the HOMO and LUMO, respectively.

are predominantly at the two bridging ligands III and IV. Moreover, the LUMO and LUMO+1 mainly arise from the two bridging ligands III and IV, while the LUMO+2 and LUMO+3 are combinations of the two nonbridging ligands I and II. The spatial overlap between HOMO and LUMO is weak. As a result, the stronger optical absorption would not correspond to the transition from HOMO to LUMO.

Table 1 gives the calculated absorption wavelengths of $[Zn(BTZ)_2]_2$ using TD-B3LYP with 6-31G* basis sets. The absorption wavelengths are predicted at 416, 363.9, 362.6, 337.3, and 281. For the absorption at 416 nm, the resultant $\pi-\pi^*$ transition from population analysis is HOMO → LUMO (23%), HOMO−1 → LUMO (48%), and HOMO−1 → LUMO+1 (45%) transition. This absorption peak shows a very low oscillator strength (*f*) of 0.0005 due to the weak spatial overlap between HOMO (or HOMO−1) and LUMO (or LUMO+1). Therefore, we should expect the stronger optical absorption observed in the experiment does not correspond to the above three electronic transitions. Frenking and co-worker also obtained a similar result that the transition from HOMO to LUMO for *mer*-Alq_3 does not result in a strong optical absorption.[22] The calculated absorption peak at 363.9 nm mainly results from the following transitions: HOMO → LUMO+2 (45%), HOMO−2 → LUMO (44%), and HOMO−1 → LUMO+3 (24%), while one at 363 nm predominantly corresponds to the HOMO−1 → LUMO+3 (48%) and HOMO−2 → LUMO (43%) transitions. According to these results and the FMO distribution of the S_0 state, we can confirm that the calculated absorption peaks at 363.9 and 362.6 nm mainly result from the charge-transfer transition within the ligands (LLCT) from the phenoxide ring of the ligands I and II to the benzothiazolate rings, accompanying a metal-to-ligand charge-transfer transition (MLCT) (3.1%). The absorption at 337.3 nm mainly corresponds to the LLCT transition from the phenoxide side of the ligands III and IV to the benzothiazolate rings as well as a small MLCT of 3.3%. The calculated absorption peaks are in good agreement with the experimental data in solution.

Analysis of the FMOs for the S_1 state shown in Figure S1 indicates that the extent of localization for the MOs is similar to that in the S_0 state. The HOMO and HOMO−1 of the S_1 state exhibit a similar MO distribution, which is localized mainly on the phenoxide sides of the two nonbridging ligands I and II. The HOMO−2 is distributed predominantly over the two bridging ligands III and IV while it also shows some MO localization on the ligands I and II. The LUMO and LUMO+1 primarily lie on the two bridging ligands III and IV, whereas LUMO+2 and LUMO+3 are localized predominantly on the two nonbridging ligands III and IV. Similar to the S_0 state, the S_1 state also shows a weak spatial overlap between HOMO and LUMO. As a result, the stronger fluorescent emission could result from the transition from LUMO to HOMO−2 rather than from LUMO to HOMO. This deduction is supported by the following calculated result. The fluorescent emission wavelengths calculated using TD-B3LYP with 6-31 G(D) basis sets are predicted at 546 and 414 nm, whose *f* data are 0.005 and 0.055, respectively (see Table S2). The electron transitions at 546 and 414 nm correspond to the transition from LUMO to HOMO and from LUMO to HOMO−2, respectively. Simultaneously, we observed that the fluorescent emission at 414 nm mainly corresponds to the charge-transfer transitions from the benzothiazolate rings of the ligands III and IV to the phenoxide side of the ligands I and II. The calculated value of 414 for the LUMO → HOMO−2 emission having the significant *f* datum can be compared with the experimental value of 455 nm in the solution.

The FMOs for the T_1 state of the $[Zn(BTZ)_2]_2$ molecule are shown in Figure S2. The FMO distribution of the T_1 state is different from those in the S_0 and S_1 states due to the large relaxation of the structure. The HOMO of the T_1 state is mainly localized on the phenoxide sides of the nonbridging ligand I while the HOMO−1 is distributed over the other nonbridging ligand II. We found that the HOMO−2 originates from the nonbridging ligand I and the bridging ligand IV, whereas the HOMO−3 is mainly localized on the ligands I, III, and IV. Both the LUMO and LUMO+1 are localized predominantly on the nonbridging ligand I and the bridging ligand III. LUMO+2 and LUMO+3 are primarily laid on the bridging ligand IV and the nonbridging ligand II, respectively. This shape of the FMOs favors the emission transition from LUMO to HOMO. The TD-B3LYP calculations for $[Zn(BTZ)_2]_2$ also provide an estimate of the relaxed emission energy from the optimized T_1 state structure to the S_0 state. The calculated phosphorescent emission is located on 536.2 nm (2.3 eV), which is in good agreement with the experimental value of 523 nm. The assignment of the T_1 → S_0 transition is as follows: LUMO → HOMO (32%), LUMO → HOMO−2 (30%), and LUMO+1 → HOMO (20%), mainly corresponding to the charge-transfer transitions between the ligands.

Charge Carrier Transport Properties. Previous works demonstrate that the dimeric molecules $[Zn(BTZ)_2]_2$ exist in the single crystal.[13] The single crystal of the zinc complex was grown from ethanol to study the effect of growing methods on the crystal structure. The crystal also exists as the anhydrous dimer $[Zn(BTZ)_2]_2$, which consists of two isotropic zinc ion centers with five-coordinate geometries. The single-crystal grown from ethanol has crystal cell parameters similar to that prepared by the sublimation method. The molecular conformation, molecular packing, bonds lengths, and bond angles are identical to our previously reported results.[13] Two ligands are involved in bridging

(22) Zhang, J. P.; Frenking, G. *J. Phys. Chem. A* **2004**, *108*, 10296.

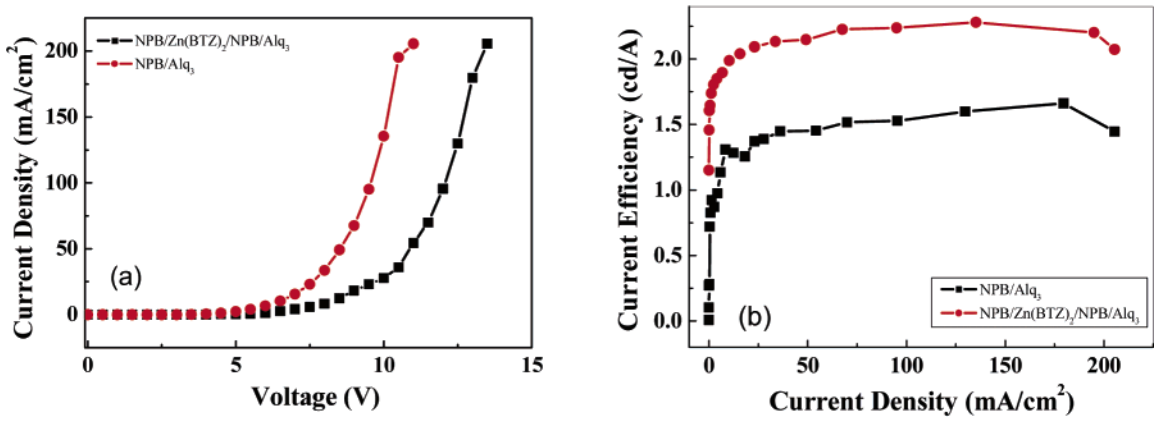

Figure 4. Current density−voltage (a) and current efficiency−current density (b) characteristics of the devices ITO/NPB/Alq_3/LiF/Al and ITO/NPB/$[Zn(BTZ)_2]_2$/NPB/Alq_3/LiF/Al.

through the phenolato oxygens, but the remaining two ligands are bound to one of the two zinc atoms only. The parallel arrangement of the nonbridging ligands on adjacent dimeric units results in a closely intermolecular $\pi-\pi$ interaction of 3.76 Å, while the intermolecular distance between the bridging ligands is 3.66 Å. The intensely intermolecular interaction would lead to good carrier transport properties. Simultaneously, the theoretical calculation for the dimeric molecule $[Zn(BTZ)_2]_2$ showed the distribution of the extra hole in the cation calculated as excess spin densities is completely localized on both nonbridging ligands. A different result was found in the anion, where the distribution of the electron is localized on all four ligands.[13] Hole and electron transports in disordered amorphous molecular solids occur via a hopping mechanism. These may be viewed as a one-hole production process of a neutral molecule concomitant with reduction of its cation and one-electron production process of the neutral molecule concomitant with oxidation of its anion. Therefore, the above results support that the complex would exhibit hole-transporting properties as well as electron-transporting characteristics. The carrier-transporting properties principally involve the ligands rather than the zinc center. Strong $\pi-\pi$ stacking between the neighboring ligands provides an efficient pathway for charge carrier transport. Electron may hop either between the two close nonbridging ligands or between the two neighboring bridging ligands, but hole transport only has one pathway hopping from the nonbridging ligand to one of the neighboring molecules. The excellent electron-transporting properties of the $[Zn(BTZ)_2]_2$ complex have been demonstrated by experimental results.[13] To study the hole-transporting characteristics, we fabricated the bilayer OLEDs based on $[Zn(BTZ)_2]_2$. The hole-transport material NPB was used for comparative purposes, while the electron-transporting and emissive layers were composed of Alq_3. The device structure was ITO/HTL(50 nm)/Alq_3(50 nm)/Al, where the HTL (hole-transporting layer) was either NPB or the zinc complex.

Direct comparison of the hole-transport properties between devices based on the bilayer $[Zn(BTZ)_2]_2$/Alq_3 and NPB/Alq_3 is not adequate due to large overlapping between PL spectra of $[Zn(BTZ)_2]_2$ and Alq_3, and different HOMO energies of $[Zn(BTZ)_2]_2$ and NPB. To obtain the emission of Alq_3 and decrease the effects of hole injection barriers, the devices ITO/NPB/Alq_3/LiF/Al and ITO/NPB/$[Zn(BTZ)_2]_2$/NPB/Alq_3/LiF/Al were prepared. All devices exhibit almost the same EL spectra with an emission peak at 513 nm, which are similar to the PL spectrum of Alq_3. This result indicates that the origin of the blue-green emission is attributed to the intrinsic emission of Alq_3. Figure 4 displays the current density−voltage and current density−current efficiency characteristics of the devices with structures of ITO/NPB/Alq_3/LiF/Al and ITO/NPB/$[Zn(BTZ)_2]_2$/NPB/Alq_3/LiF/Al. At a given bias, a smaller amount of current was passed through the $[Zn(BTA)_2]_2$ device compared to the standard NPB device. Analogous behavior was also observed for devices using an Al cathode, which show higher operation voltage compared with the devices using the LiF/Al cathode. Our results indicate that $[Zn(BTZ)_2]_2$ complex exhibits a hole-transport property. Smaller current obtained for the devices based on $[Zn(BTZ)_2]_2$ complex is due to a hole-transport mobility lower than that of the NPB[23] as well as the hole-injection barrier at the $[Zn(BTZ)_2]_2$/NPB interface.[13] We observed that introduction of the $[Zn(BTZ)_2]_2$ improves the current efficiency from 1.66 to 2.28 cd/A, increasing the turn-on voltage from 4.6 to 5.63 V. We could suggest that the $[Zn(BTZ)_2]_2$ interlayer plays an important role in improving the balance of electron and hole current and hence enhancing the current efficiency. As is well-known, electrons are the minor carriers and holes are the major ones in the NPB/Alq_3 devices because the hole mobility of NPB is 2 orders of magnitude higher than that of the electrons for Alq_3. Accordingly, it leads to an unbalance of holes and electrons, which is unhelpful to enhance the luminance efficiency. As a result, reducing the number of holes in the hole-transporting layer generally helps to improve the electron−hole balance in the NPB/Alq_3 devices. The inserting of the $[Zn(BTZ)_2]_2$ layer with a poor hole-transporting properties into the NPB layer can decrease the number of holes reaching the Alq_3 layer, leading to the balanced charge carrier transport process. Therefore, to achieve the same current density in the OLEDs, the applied voltage is increased. The improvement on current efficiency is mainly attributed to the reduction of the number of holes in the OLEDs.

Charge-Transfer Integral and Reorganization Energies. For the sake of an extensive explanation of the reason why

(23) Yasuda, T.; Yamaguchi, Y.; Fujita, K.; Tsutsi, T. *Chem. Lett.* **2003**, *32*, 644.

the dimer $[Zn(BTZ)_2]_2$ exhibits higher electron mobility than hole mobility,[23] the theoretical study of the transporting properties was performed. At room temperature, the charge carrier mobility for most of the organic materials is often determined by a thermally activated hopping transport process, which can be depicted as an electron or hole transfer reaction, i.e., an electron or hole is transferred from one molecule to the neighboring one.[24] The rate of intermolecular electron or hole hopping is dictated both by the charge transfer integral (H_{ad}), which needs to be maximized, and by the reorganization energy (λ_{reorg}), which needs to be small for efficient charge transport, due to geometric relaxation. Both H_{ad} and intramolecular λ_{reorg} can be evaluated by quantum chemical calculation. Recently, Marks and co-workers studied the hopping transport in conductive heterocyclic oligomers and substituent effects on the reorganization energies.[24b] The charge-transporting properties of *mer*-Alq_3 have been investigated by quantum chemical calculations.[24a] The reason why Alq_3 exhibits higher electron mobility than hole mobility results from the fact that H_{ad}'s for electron transport are more than 10 times greater than those for hole transport.

We calculated the H_{ad} of $[Zn(BTZ)_2]_2$ by employing Koopmans theory in conjunction with Hartree−Fock model (HF−KT). A first step toward calculating H_{ad} for $[Zn(BTZ)_2]_2$ in an amorphous film is to confirm the relative positions of the two molecules in the hopping complexes. Within a microscopic range, an amorphous material can be considered as many molecules with relative positions similar to those in the crystalline state. $[Zn(BTZ)_2]_2$ has a space group $P\bar{1}$, while each unit cell shows one molecule. An electron or hole on the $[Zn(BTZ)_2]_2$ molecule can hop to others related by either translational or inversion symmetry in the neighboring unit cell. We chose 14 charge hopping pathways between two neighboring $[Zn(BTZ)_2]_2$ molecules to calculate the charge-transfer integral (see Figure S3). The pathways I−VI were obtained by operation of translational symmetry in the neighboring unit cells, while the pathways VII−XIV were gained by operation of inversion symmetry in addition to operation of translational symmetry. We calculated both the electron and hole coupling energies at HF/6-31g(d) level performed by Gaussian 03. Energy splitting values were calculated as the energy differences between LUMO and LUMO+1 (for electron transfer) or between HOMO and HOMO−1 (for hole transfer) of the hopping complex. H_{ad} is half of the energy splitting.

The transfer integrals H_{ad}'s in all pathways are in the range $10^{-5}-10^{-1}$ eV (see Table S3). The magnitudes of H_{ad}'s depend on the overlap degree between the LUMOs or HOMOs of the hopping complex. When the Zn−Zn distance between the hopping partners is short, there is good overlap of orbitals and consequently large H_{ad} values, such as in the pathways I, II, III, and IV. Simultaneously, it is found that the type of the molecular contacts in the hopping partners have a great contribution to the H_{ad} values. Both the two parallel nonbridging ligands in pathways I and II and the two parallel bridging ligands in pathways III and IV have close intermolecular $\pi-\pi$ interaction, leading to the two largest $H_{ad}(h)$ and $H_{ad}(e)$ values. The $H_{ad}(e)$ value in pathways I and II is the largest among all the H_{ad}'s for electron transport, while a similar result for $H_{ad}(h)$ was also obtained. The parallel bridging ligands in pathways III and IV lead to the second largest H_{ad} values. The largest $H_{ad}(h)$ and $H_{ad}(e)$ have almost the same values. Consequently, the hole mobility is predicted to be close to the electron mobility, apparently contradicting the experimental observations. This suggests that the charge-transfer integral λ_{reorg} must influence charge transport in a major way.

We carried out DFT-B3LYP calculations on $[Zn(BTZ)_2]_2$ for λ_{reorg} employing a 3-21 G* basis set using the Gaussian 03 program suite. For comparison, we also calculated λ_{reorg} for the *mer*-Alq_3 molecule using the same calculation method. Our calculation results give $\lambda_{reorg}(e)$ of 0.27 eV and $\lambda_{reorg}(h)$ of 0.24 eV for the *mer*-Alq_3 molecule. These data are compared to those reported by Hsu and co-workers.[24a] Interestingly, the $[Zn(BTZ)_2]_2$ molecule exhibits both the smaller $\lambda_{reorg}(e)$ (0.11 eV) and $\lambda_{reorg}(h)$ (0.17 eV) than those of the *mer*-Alq_3 molecule. To obtain the high charge-transfer rate, the reorganization energies need to be kept as low as possible. Therefore, the smaller $\lambda_{reorg}(e)$ value for the $[Zn(BTZ)_2]_2$ molecule would suggest that $[Zn(BTZ)_2]_2$ would be a better electron transporter than a hole transporter. This deduction is consistent with the experimental results.

Recently, Bromley et al. reported that the molecular packing is a key factor in assessing hopping mobilities.[25] The local environmental steric packing of the nearest neighboring (*NN*) molecules may play an important role in lowering λ_{reorg}. Our above reorganization energies calculated with respect to the isolated molecules exclude the electronic coupling between the adjacent molecules. Herein, we further calculated λ_{reorg} of the $[Zn(BTZ)_2]_2$ molecule embedded by four *NN* molecules, which were fixed at the geometry of the single crystal. This entails a stack of five molecules along both *b* and *a* crystal axes to take in the primary charge-transport direction in the crystal (see Figure S4). In the case of the embedded molecule, we obtained the $\lambda_{reorg}(e)$ of 0.067 eV and $\lambda_{reorg}(h)$ of 0.116 eV, which are 39% and 32% lower than those of the isolated molecule, respectively. This result indicates that the local intermolecular interactions can have a strong influence on the λ_{reorg} values, similar to the result obtained for dithiophene-tetrathiafulvalene.[25] Compared to the isolated molecule, the embedded $[Zn(BTZ)_2]_2$ molecule exhibits an obviously lower $\lambda_{reorg}(e)$ value than that of $\lambda_{reorg}(h)$. Therefore, the λ_{reorg} value calculated for the embedded $[Zn(BTZ)_2]_2$ molecule would provide more persuasive evidence for its electron-transporting properties compared to the hole-transporting properties.

(24) (a) Lin, B. C.; Cheng, C. P.; You, Z. Q.; Hsu, C. P. *J. Am. Chem. Soc.* **2005**, *127*, 66. (b) Hutchison, G. R.; Ratner, M. A.; Marks, T. J. *J. Am. Chem. Soc.* **2005**, *127*, 2339. (c) Lin, B. C.; Cheng, C. P.; Lao, Z. P. M. *J. Phys. Chem. A* **2003**, *107*, 5241. (d) Brédas, J. L.; Calbert, J. P.; da Silva, D. A.; Cornil, J. *Proc. Natl. Acad. Sci.* **2002**, *99*, 5804. (e) Cornil, J.; Beljonne, D.; Calbert, J. P.; Brédas, J. L. *Adv. Mater.* **2001**, *13*, 1053. (f) Epstein, A. J.; Lee, W. P.; Prigodin, V. N. *Synth. Met.* **2001**, *117*, 9. (g) Reedijk, J. A.; Martens, H. C. F.; van Bohemen, S. M. C.; Hilt, O.; Brom, H. B.; Michels, M. A. J. *Synth. Met.* **1999**, *101*, 475.

(25) Bromley, S. T.; Torrent, M. M.; Hadley, P.; Rovira, C. *J. Am. Chem. Soc.* **2004**, *126*, 6544.

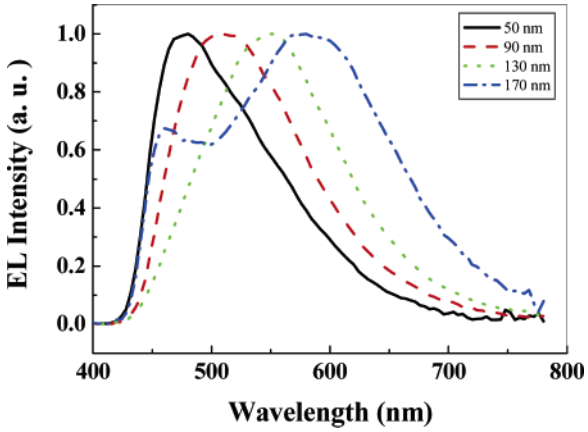

Figure 5. EL spectra of the devices with the structure of ITO/F_{16}CuPc-(5.5 nm)/$[Zn(BTZ)_2]_2$/Al for the various $[Zn(BTZ)_2]_2$ thicknesses.

Electroluminescence. The $[Zn(BTZ)_2]_2$ complex is an outstanding white EL material. Some research groups have already reported the EL properties of the complex.[12,20,26] Broad EL spectra were observed in the bilayer OLEDs used *N*,*N*′-diphenyl-*N*,*N*′-di(3-methylphenyl)-1,1′-biphenyl-4,4′-diamine (TPD) and $[Zn(BTZ)_2]_2$ as the hole-transporting and emissive layers, respectively. However, the origin of broad EL emission is still not well understood. In the bilayer OLEDs, exciplex formation between the hole-transporting material and $[Zn(BTZ)_2]_2$ could be contributive to the broadening of the EL spectra. To obtain the real origin of the unusually broad EL emission and remove the effect of exciplex, we fabricated the devices with a structure of ITO/F_{16}CuPc(5.5 nm)/$[Zn(BTZ)_2]_2$/Al. We have demonstrated that using an ultrathin F_{16}CuPc layer can significantly enhance hole injection and increase EL efficiency.[27] Figure 5 shows the EL spectra of these devices for the various $[Zn(BTZ)_2]_2$ thicknesses. We observed a striking difference between the EL and PL spectra. The EL spectra are strongly dependent on the thickness values of the $[Zn(BTZ)_2]_2$ layer. A similar result was obtained for the bilayer devices based on TPD and $[Zn(BTZ)_2]_2$.[20] The important difference between the results presented here and their works is that our devices contain no hole-transport layer. When the thickness of the $[Zn(BTZ)_2]_2$ layer is 50 nm, the EL spectrum has a peak at about 477 nm and a relatively long tail toward the red. The full-width at half-maximum (fwhm) of the spectrum is about 117 nm in this thickness. Increasing the thickness of the $[Zn(BTZ)_2]_2$ layer results in a systematic red shift in the peak positions of the EL spectra and broadening of the EL spectra. As the thickness of the $[Zn(BTZ)_2]_2$ layer increases to 170 nm, the EL spectrum splits into two peaks located at 458 and 580 nm, respectively. This spectrum exhibits a fwhm of 220 nm, covering the main part of the visible range from 420 to 780 nm. The EL spectra of OLEDs for the various thicknesses do not show any significant variation with applied bias.

The EL spectra of Alq_3-based OLEDs were measured as a function of the thickness of the emissive layer.[28] Microcavity effects provided sufficient explanation for the observed phenomena. In a microcavity device, optical interference effects can significantly alter the EL spectrum. Moreover, the microcavity OLEDs typically exhibit an important blue shift with the viewing angles.[29] To investigate the origin of our observed features in more detail, we measured the EL spectra of the devices ITO/F_{16}CuPc(5.5 nm)/$[Zn(BTZ)_2]_2$/Al at the different viewing angles (see Figure 6). For small $[Zn(BTZ)_2]_2$ thickness of 50 nm, no significant variation of the EL spectra was achieved with the viewing angles. A thicker $[Zn(BTZ)_2]_2$ layer results in an obvious blue shift with the viewing angles. At 0° viewing angle, the EL spectrum for the $[Zn(BTZ)_2]_2$ thickness of 170 nm exhibits two emission peaks located on about 460 and 580 nm, whereas at a larger viewing angle the longer wavelength emission peak shows a pronounced blue shift and intensity of the shorter wavelength emission peak decreases. The previous works demonstrated that a noncavity OLED would show no significant change in the emission spectra with the viewing angles.[1,2] Therefore, we can expect that optical interference effect is the main origin of the broad light emission for the devices based on $[Zn(BTZ)_2]_2$.

Additionally, phosphorescence of $[Zn(BTZ)_2]_2$ may also contribute to the broad emission in the $[Zn(BTZ)_2]_2$ emitting devices because phosphorescence was detected in the case of photoexcitation for the $[Zn(BTZ)_2]_2$ thin film at 77 K. This proposal was supported by the emission lifetimes, which were determined by the turn-off behavior of the EL devices using the transient EL method. To measure the emission lifetimes, we fabricated the devices with a structure of ITO/MoO_3/$[Zn(BTZ)_2]_2$/Al. We also obtained a broad light emission for the above devices. The light emission decays biexponentially with lifetimes of ca. 60−350 ns and 1.33−1.46 μs, indicating that the emission involves two components. The emission with the shorter lifetime may be ascribed to the delayed fluorescence generated by triplet−triplet annihilation. The observed longer lifetime in the microsecond range suggests that it arises from a triplet parentage of $[Zn(BTZ)_2]_2$. Therefore, we can assign this emission with lifetimes of ca. 1.33−1.46 μs to the phosphorescence of $[Zn(BTZ)_2]_2$. Our above results indicate that the EL spectra vary strongly with the thicknesses of the emissive layer. Optical interference effects and light emission originating from both fluorescence and phosphorescence can explain all of the observed phenomena. In the OLED, electrons and holes are injected from the cathode and anode, respectively, under application of an electric field. The injected carriers transport within the $[Zn(BTZ)_2]_2$ layer and recombine to

(26) (a) Kwon, O. K.; Kim, Y. K.; Sohn, B. C.; Ha, Y. K. *Mol. Cryst. Liq. Cryst.* **2000**, *349*, 405. (b) Singh, S. P.; Mohapatra, Y. N.; Qureshi, M.; Manoharan, S. S. *Appl. Phys. Lett.* **2005**, *86*, 113505.
(27) Di, C. A.; Yu, G.; Liu, Y. Q.; Xu, X. J.; Song, Y. B.; Zhu, D. B. *Appl. Phys. Lett.* **2006**, *89*, 033502.
(28) (a) So, S. K.; Choi, W. K.; Leung, L. M.; Neyts, K. *Appl. Phys. Lett.* **1999**, *74*, 1939. (b) Cheung, C. H.; Djurišić, A. B.; Kwong, C. Y.; Tam, H. L.; Cheah, K. W.; Liu, Z. T.; Chan, W. K.; Chui, P. C.; Chan, J.; Rakić, A. D. *Appl. Phys. Lett.* **2004**, *85*, 2944. (c) Shore, J. D. *Appl. Phys. Lett.* **2005**, *86*, 186101.
(29) (a) Dodabalapur, A.; Rothberg, L. J.; Jordan, R. H.; Miller, T. M.; Slusher, R. E.; Phillips, J. M. *J. Appl. Phys.* **1996**, *80*, 6954. (b) Dirr, S.; Wiese, S.; Johannes, H. H.; Ammermann, D.; Böhler, A.; Grahn, W.; Kowalsky, W. *Synth. Met.* **1997**, *91*, 53. (c) Jordan, R. H.; Rothberg, L. J.; Dodabalapur, A.; Slusher, R. E. *Appl. Phys. Lett.* **1996**, *69*, 1997.

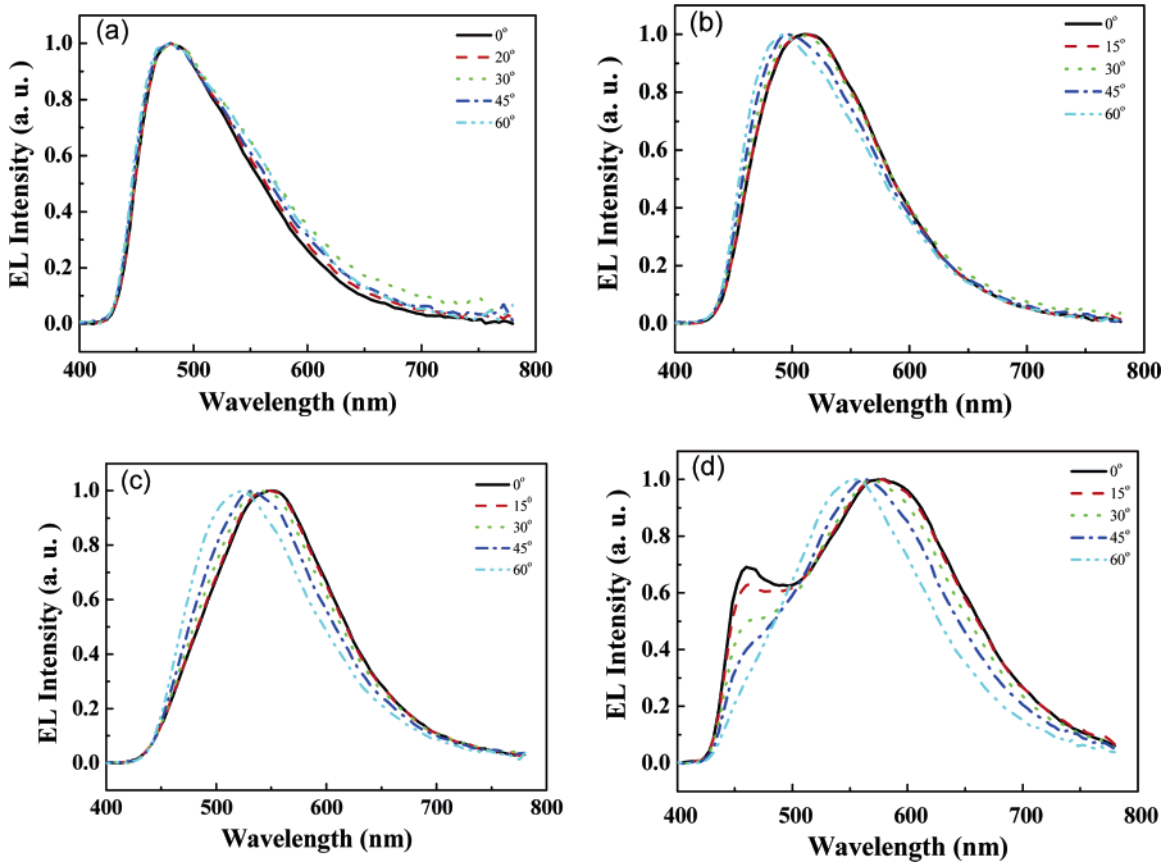

Figure 6. EL spectra at different viewing angles for the ITO/F_{16}CuPc(5.5 nm)/$[Zn(BTZ)_2]_2$/Al devices with the $[Zn(BTZ)_2]_2$ thicknesses of 50 (a), 90 (b), 130 (c), and 170 (d) nm, respectively.

produce singlet and triplet excitons. The emission from the singlet and triplet excitons generates a short-wavelength fluorescence and long-wavelength phosphorescence, respectively. The metallic cathode can reflect the radiated light from the organic layer. When the directly radiated and reflected waves add up, the optical interference is expected to be dominant. The most important interference effect occurs between light emitted directly out of the device through the glass substrate and that reflected off the metallic cathode. The reflections at the ITO anode and the glass substrate also result in smaller contributions. The resulting emission spectrum can be expressed as the product of the innate fluorescent and phosphorescent emission of $[Zn(BTZ)_2]_2$ and the optical response of the device. As a result, the $[Zn(BTZ)_2]_2$ device could exhibit a broad EL spectrum, which is a function of the thicknesses of the emissive layer.

Conclusions

We present theoretical and experimental studies of charge carrier transporting and photophysical characteristics for the $[Zn(BTZ)_2]_2$ chelate. Quantum chemical calculations demonstrated that $[Zn(BTZ)_2]_2$ is a better electron transporter than a hole transporter. The $[Zn(BTZ)_2]_2$ films show an orange phosphorescent emission at 77 K. We calculated the absorption and emission wavelengths using the optimized geometries of the S_0, S_1, and T_1 states, respectively. The optical interference effects and photosphorescent emission were observed for the devices with a structure of ITO/F_{16}CuPc(5.5 nm)/$[Zn(BTZ)_2]_2$/Al. The EL spectra of the devices depend strongly on the thicknesses of the $[Zn(BTZ)_2]_2$ layer. A broad light emission with a fwhm of 220 nm was obtained.

Acknowledgment. The authors thank Drs. H. W. Ma and Y. Li for X-ray analysis. This work was supported by the Major State Basic Research Development Program, the National Natural Science Foundations of China (20573115, 90206049, 20472089, 20421101, 60671047), and the Chinese Academy of Sciences.

Supporting Information Available: The results of quantum chemical calculations. This material is available free of charge via the Internet at http://pubs.acs.org.

CM062960B